Revisiting the use of electrolyte additives in Li-S batteries: Role of porosity of sulfur host materials

Journal:	*Sustainable Energy & Fuels*
Manuscript ID	SE-ART-05-2019-000277.R1
Article Type:	Paper
Date Submitted by the Author:	23-Jul-2019
Complete List of Authors:	Singh, Arvinder; Drexel University, Chemical and Biological Engineering Rafie, Ayda; Drexel University, Chemical and Biological Engineering Kalra, Vibha; Drexel University, Chemical and Biologial Engineering

Revisiting the use of electrolyte additives in Li-S batteries: Role of porosity of sulfur host materials

Arvinder Singh, Ayda Rafie and Vibha Kalra*

Chemical and Biological Engineering, Drexel University, Philadelphia-19104, USA

*Email: vk99@drexel.edu, Phone: +1 (607) 592-5037

Abstract

In this work, we demonstrate the important role of porosity of the sulfur host material for the efficient functioning of the biphenyl-4,4'-dithiol (BPD) electrolyte additive in Li-S batteries. We compare the electrochemical performance of Li-S cells fabricated using non-porous (CNFs), micro-porous (mi-CNFs), and micro-meso porous carbon nanofibers (me-CNFs) as sulfur hosts. The me-CNFs/S cathodes exhibit a stable specific capacity with 83% capacity retention at C/2 after 200 cycles and 90% retention at C/5 after 150 cycles, whereas mi-CNFs/S and CNFs/S cathodes retain close to only 30% capacity after 200 cycles. We investigate the role of porosity using two approaches- Li^+ diffusion coefficient and shuttle-current measurements. The me-CNFs/S cathodes show a relatively higher Li^+ ion diffusion coefficient during reduction and oxidation processes thus

indicating a low concentration of BPD-S_x^{2-} species into the electrolyte. Further, the me-

CNFs/S cathodes indicate a relatively lower shuttle effect compared to the other two

cathodes further validating the presence of a lower concentration of polysulfides in the

electrolyte. Based on the size of BPD-S_x^{2-} complex, we infer that the use of mesoporous

me-CNFs is essential for achieving long-term cycling. Our results show that the

integration of suitable porous host materials with functional electrolyte additives presents

a promising approach for developing high-performance Li-S batteries.

Introduction

The capacity of advanced insertion cathode and anode materials available for Li-ion

batteries is nearing physical limitations. Therefore, Li-ion batteries may not ever meet the

targeted 500 km range/per charge within reasonable weight (~200 kg) and cost.[1-4]

Consequently, several other secondary battery (e.g., Li-sulfur, Li-air, and Na-air)

chemistries are attracting considerable attention as possible high-energy-density

alternatives.[5] Among all, lithium-sulfur (Li-S) batteries are getting prominence because of

their potential to achieve 3-4 times higher device-level energy density at a relatively low

cost in comparison to Li-ion batteries.[6] The high energy density of Li-S batteries relies on

the high capacity ($\sim$1675 mAh g^{-1}) of cost-effective, abundant and environmentally benign

elemental sulfur.[3] However, commercialization of Li-S batteries is hampered due to

chronic technological issues imposed by various complicated steps involved in the

(de)lithiation process of elemental sulfur.[4] These practical issues include low sulfur

utilization and coulombic efficiency, shuttling of intermediate lithium polysulfides (Li_2S_n,

4$\leq$n$\leq$8), and mechanical failure of sulfur-based cathodes.[7] Of the approaches to address

these challenges, most are devoted to designing nanostructured conducting host

materials.[8] These host materials for sulfur not only supply electrons during redox

processes but also suppress shuttling of intermediate lithium polysulfides through

physical (adsorption) or chemical interactions (e.g., chemisorption, Lewis acid-base).[1, 6]

Significant progress has been witnessedin the recent past in Li-S batteries with the use

of various host materials such as carbonaceous (e.g., graphene, CNTs, porous carbon,

carbon nanofibers)[1, 3, 6] materials, metal oxides (e.g., TiO_2, ZnO, MgO)[9], metal organic

frameworks[10], and polymers (e.g., polyaniline)[11].

Another promising approach, over-shadowed by advancement in cathode architectures, is the modification of the electrolyte with functional additives.[12] Additives not only can tune the dissolution of polysulfides but also can modify the electrolyte/electrode interface on Li- anode. Therefore, additives can play an essential role in improving the cycle life of Li-S batteries.[12-13] Various additives including Li salts and organic molecules have been used not only to alleviate the shuttle problem but also to protect Li anode by forming stable solid electrolyte interphase (SEI) layer.[12-16] Lithium nitrate (LiNO$_3$) is the most common additive in Li-S batteries which inhibits the continuous Li$_2$S$_2$/Li$_2$S deposition on the Li-anode by forming a stable SEI layer.[12-13] However, in most cases, LiNO$_3$ does not yet provide long-term protection to Li anodes due to its continuous consumption at both anodes and cathodes and presence of defects within the SEI layer.[12-13]

Several other additives such as P$_2$O$_5$, LiI, polysulfides, dimethyl disulfide (DMDS), lithium azide, LiBr have been explored which either form complexes with intermediate polysulfides (PS) to suppress their dissolution and shuttle or protect Li anode *via* stable SEI layer.[15, 17-19] For example, F. Wu *et al.* reported better cycle life of Li-S cells with the

use of LiI as an additive, which formed iodine-containing protective layers on the cathode

and anode sides to suppress shuttling.[19] Recently, H. –L., Wu *et al.* reported the use of

biphenyl-4,4'-dithiol (BPD) as a promising additive in Li-S batteries to improve their cycle

life.[20] Authors found that the BPD-short chain polysulfide (BPD-S_x^{2-}; 1≤x≤4) complexes

formed during charge-discharge processes not only modified the kinetics of the formation

of short-chain polysulfides but also reduced the polysulfide dissolution.[20] It is evident from

the above discussion that additives are crucial as they can alter the redox reaction

pathways, the viscosity of electrolytes, dissolution of intermediate polysulfides *via*

complex formation and SEI functionality for boosting the performance of Li-S batteries.[17-20] However, it is worth noting that in all these abovementioned studies, slurry based

standard carbon/S cathodes are used, and the importance of the design of the host

material is undervalued.[17-20] The reported standard carbon/S cathodes with additive

based electrolytes inevitably involve the unsought diffusion of complex polysulfide-

additive species into the electrolyte. The diffusion of such complex species results in the

deposition of Li_2S/Li_2S_2 at the Li-anode, which ultimately undermines the cycle life of Li-

S cells. One possible way to achieve optimal performance in additive based Li-S batteries

is to use high surface area host materials with suitable porosity simultaneously. An ideal

porous host material would be able to accommodate the large-sized polysulfide-additive

complexes and prevent their undesired diffusion into the electrolyte. Therefore, a

combination of suitable porous host materials with electrolyte additives would be a more

promising approach to benefit the cycle life of Li-S cells.

In this work, we attempt to highlight the importance of appropriate pore sizes and

high surface area of carbon nanofiber serving as a sulfur host material for the efficient

functioning of the biphenyl-4,4'-dithiol (BPD) additive in Li-S batteries. To elucidate the

effect of porosity, we used binder-free, free-standing carbon nanofibers as model sulfur

host materials. It is because the porosity of the host material in slurry based cathodes is

uncomprehended after the addition of binders and conducting additives. We prepared

three types of sulfur cathodes using non-porous carbon nanofibers (CNFs/S),

microporous carbon nanofibers (mi-CNFs/S) and micro-mesoporous carbon nanofibers

(me-CNFs/S) with 47-53 wt% (1.3-1.5 mgcm^{-2}) sulfur loading. The Li-S cells fabricated

with me-CNFs/S cathodes exhibit a high specific capacity of ~561mAh g^{-1} over 200 cycles

at C/2 rate in BPD additive based ether electrolyte. In contrast, Li-S cells fabricated using

mi-CNFs/S and CNFs/S cathodes show only ~319 mAh g^{-1} and ~230 mAh g^{-1} capacity after 200 cycles, respectively. We used two approaches- Li$^+$ diffusion coefficient and shuttle-current measurements to experimentally investigate the critical role of porosity of carbon nanofiber host materials. The me-CNFs/S cathodes show a relatively higher Li$^+$ ion diffusion coefficient during reduction and oxidation processes than CNFs/S, and mi-CNFs/S cathodes in BPD added electrolyte. The observed faster Li$^+$ diffusion manifests a large contact area between the me-CNFs host material and BPD-S$_x^{2-}$ complexes for their adsorption and a low concentration of these complex species into the electrolyte. Moreover, we observe a relatively lower shuttle current for theme-CNFs/S than mi-CNFs/S cathodes in BPD added electrolyte which again indicates a lower shuttle effect in me-CNFs/S based Li-S cells. Based on the size of BPD-S$_x^{2-}$ complexes, we infer that use of mesoporous me-CNFs (vs. micro- or non-porous CNFs) is indispensable for accommodating BPD-polysulfide complexes (anions) and minimizing their shuttling. Our work shows that integrating suitable porous host materials with additive based electrolyte would be a more promising approach for developing high-performance Li-S batteries.

Experimental Methods

Fabrication of CNFs, mi-CNFs, andme-CNFs

CNFs, mi-CNFs and me-CNFs samples were prepared using electrospinning technique followed by carbonization as reported elsewhere by our group.[21-22] In brief, 10 wt% polyacrylonitrile (PAN, M.W. 150000, Sigma-Aldrich) was dissolved in N, N-dimethylformamide (DMF, Sigma Aldrich) at room temperature and stirred for 4–5 h. The nanofibers were electrospun at room temperature using a 22-gauge stainless steel needle (Hamilton Co.) with ~15 cm distance between the needle tip and the grounded collector (aluminum foil). The applied voltage was ~10 kV, and humidity was below 20%. The electrospun nanofibers were first stabilized in air at 280°C for 6 h and then carbonized at 1000°C (heating rate of 2°C/min) for 1h in a horizontal tube furnace under steady nitrogen flow to get CNFs. To prepare mi-CNFs, stabilized electrospun nanofibers were first heated up to 900°C (heating rate of 2.5°C/min) in steady-state nitrogen flow and then activated with the CO_2 flow for 1 h at 900°C. For me-CNFs, we dissolved PAN and Nafion powder (dried LIQUION 1105 purchased from Ion Power Inc.) in DMF in a 40:60 wt% ratio with a total solid concentration of ~18%. Other electrospinning and carbonization conditions were kept similar to those for the preparation of CNFs.

Physical Characterizations

We used the Field Emission Scanning Electron Microscope (FE-SEM) (Zeiss Supra 50 VP) equipped with an energy dispersive spectrometer (EDS; Oxford) for microstructural/morphological features and elemental mapping. Thermogravimetric analysis for CNFs/S, mi-CNFs/S and me-CNFs/S samples were performed on a TA Instruments 2950 (TA Instruments, New Castle, DE) under steady Ar gas flow at a heating ramp rate of 2.5°C/min. Nitrogen (N_2) adsorption-desorption analysis of CNFs, mi-CNFs, and me-CNFs samples was

carried out at 77 K with an automated gas sorption analyzer (AutoSorb iQ2, Quantachrome Instruments). Samples were degassed overnight at 200°C under N_2 flow before this measurement. The surface area (S_{BET}) and pore volumes (V_t – total pore volume; V_{micro} – micropore volume) were determined from N_2 adsorption at 77K using a density functional theory (DFT) model.

Li-S cells fabrication and electrochemical testing

We used commercial sulfur (Sigma, 100 mesh) powder for the cathode preparation without further treatment. The CNFs, mi-CNFs and me-CNFs nanofiber mats were punched (with 11 mm diameter punch) into discs and infiltrated with ~47-53 wt% (1.3-1.5 mg cm^{-2}) sulfur using rapid sulfur melt infiltration technique we developed in our lab to prepare final CNFs/S, mi-CNFs/S, and me-CNFs/S cathodes.[23] In brief, a desired amount of sulfur was sprinkled on the top of the punched electrode and then heat pressed at 155°C for 50 seconds at a mild pressure (≤250 psi). We flipped all the cathodes so that the sulfur-infusion side of cathodes was facing away from the separator. The CR2032 (MTI Corporation) coin-type Li-S cells were assembled using lithium foil anodes (Aldrich; 11 mm diameter), CNFs/S, mi-CNFs/S or me-CNFs/S cathodes (~0.855 cm^2 area), a polypropylene separator (Celgard 2500; 19 mm diameter), nickel foam (MTI corporation) spacer and 30 µL electrolyte. The electrolyte was prepared using 1.85 M $LiCF_3SO_3$ (Acros Organics), and 0.1 M $LiNO_3$ (Acros Organics) salts in a mixed solution of 1,2-dimethoxyethane (DME, Acros Organics) and 1,3-dioxolane (DOL, Acros Organics) at a 1:1 volume ratio. To modify the electrolyte, 5 mg (~25 mmol) BPD was added to 1 mL of the blank electrolyte. All assembled coin cells were held at rest at their open circuit potential for 3 hours to equilibrate them before running electrochemical experiments. Cyclic voltammetry at different scan rates between voltage 1.8-2.6 V and electrochemical impedance spectroscopy (EIS) in the frequency

range of 0.01 Hz and 100 kHz with an ac perturbation of 5 mV amplitude were performed using a potentiostat (Gamry reference 1000). Prolonged cyclic stability tests were carried out with a MACCOR (4000 series) battery cycler at different C-rates (where 1C = 1675 mAh g^{-1}) between voltage 1.8-2.6V. Li-S cells were conditioned during the first cycle at the 0.1C rate before cycling them at the 0.2C rate. Similarly, we conditioned Li-S cells at 0.1C and 0.2C rates, respectively for the first and second cycles before their prolong cycling at the 0.5C rate. The specific capacity values were calculated based on the sulfur weight in the cathode. We measured steady-state shuttle currents for mi-CNFs/S and me-CNFs/S cathodes during the 3rd charging process (3rd cycle after two full cyclic voltammetry scans) by holding Li-S cells at ~2.3 V. We hold Li-S cells at this potential for ~30 minutes to equilibrate cells. Following this, the current applied to Li-S cells was observed for 1 h at the measured open circuit voltage. This recorded steady-state current is the shuttle current. We used BPD modified electrolyte for shuttle-current measurements without lithium nitrate.

Results and Discussion

We prepared three different samples of carbon nanofibers viz., CNFs, mi-CNFs, and me-CNFs using the electrospinning technique as described in the experimental section. Figure 1(a-c) shows the SEM images of the three samples. SEM images show that all three nanofiber samples are macroscopically alike and exhibit carbon nanofibers (diameter between 200-400 nm) with a smooth surface. The 3D architecture of these free-

standing carbon nanofibers exhibits macro-sized inter-fiber spacing/voids in all three
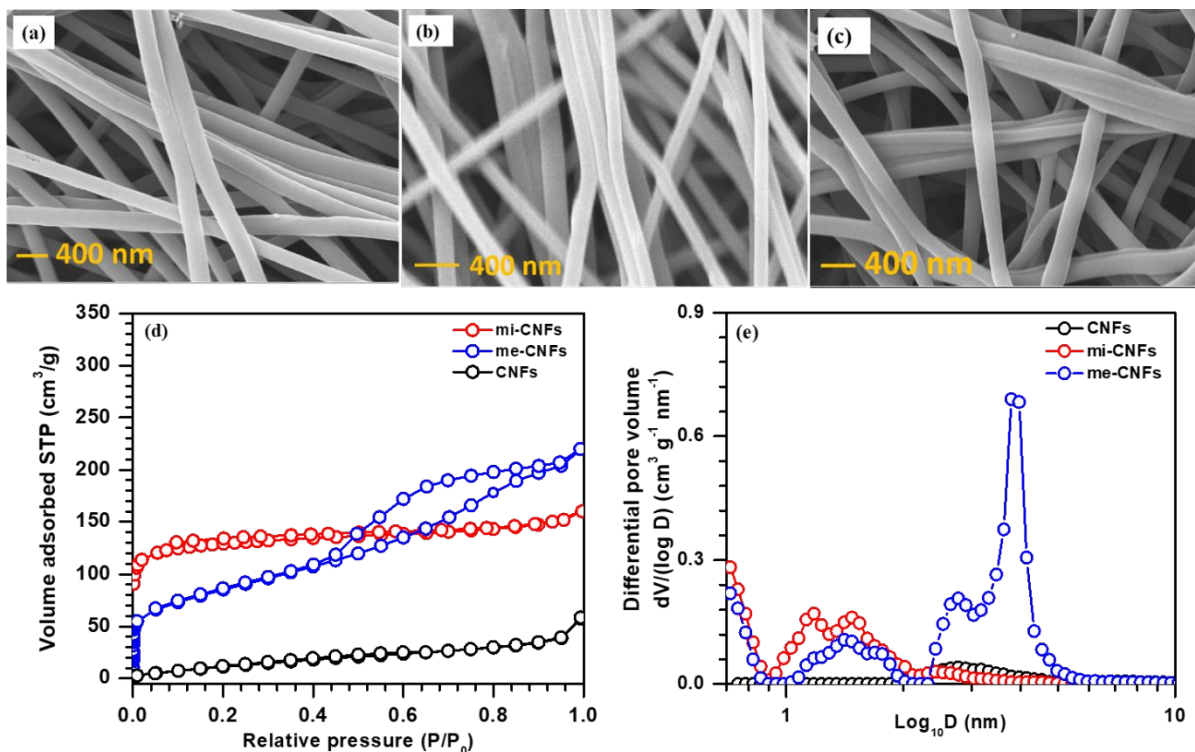
samples.

Fig. 1 SEM images of (a) CNFs, (b) mi-CNFs, and (c) me-CNFs; (d) BET N_2

adsorption-desorption curves and (e) pore size distributions for CNFs, mi-CNFs, and

me-CNFs samples.

Further, we used N_2 adsorption experiments to evaluate pore structures and surface

areas of CNFs, mi-CNFs, and me-CNFs samples. Figure 1(d) and 1(e) show Brunauer–Emmett–

Teller (BET) N_2 adsorption-desorption curves and pore size distributions for CNFs, mi-CNFs, and

me-CNFs samples. Both the CNFs and mi-CNFs samples display type I isotherm with a

constant amount of the adsorbed gas at nearly all relative pressures. This behavior

indicates the microporous structure of CNFs and mi-CNFs samples.[21, 24] After CO_2

activation, the mi-CNFs sample shows an increased amount of the adsorbed gas, which indicates

substantially improved microporosity in the sample. In contrast, the me-CNFs sample exhibits

type IV isotherm with a slowly increasing amount of the adsorbed N_2 gas at a high relative

pressure. The me-CNFs sample shows a hysteresis at a relative pressure between 0.4-

0.6, which suggests the presence of a significant fraction of slit-shaped mesopores in the

sample.[21, 24] The surface area (S_{BET}) and pore volumes (V_t – total pore volume and V_{micro}

– micropore volume) were determined from N_2 desorption at 77K using a density

functional theory (DFT) model.[24-25] According to IUPAC, pores with size <2nm are known

as micropores, pores between 2-50 nm are mesopores and pores >50 nm are known as

macropores. The CNFs sample is mostly non-porous. As seen in figure 1(e), mi-CNFs

sample, after CO_2 activation, has a considerably improved microporosity with the majority

of pores close to 1 nm and between 1-2 nm but less than 2 nm. In contrast, the me-CNFs

sample exhibits micro-/meso-porosity with lower micropore volume and substantially

larger mesopore volume with mesopores of 2.7 and 3.9 nm sizes. The mesoporosity of

the me-CNFs sample mainly results from the decomposition of the sacrificial Nafion

polymer during carbonization. The calculated total pore volume for me-CNFs, mi-CNFs,

and CNFs samples are ~0.586, ~0.324 and ~0.088 cm^3g^{-1}, respectively. The CNFs sample

exhibits a low surface area of ~54 m^2 g^{-1} since it is mostly non-porous. After activation with CO_2,

the mi-CNFs sample shows a surface area of ~459 m^2 g^{-1}. While mi-CNFs samples contain

largely micropores, the me-CNFs sample possesses a combination of both micropores

and small mesopores (≤5 nm). The me-CNFs sample has a little higher surface area of ~679

m^2 g^{-1}. As reported in our previous paper, these three CNFs have no significant difference in the

surface elemental composition as well as the surface functionalities.[22] The performance of Li-S

cells using these different CNFs materials will not be influenced by the surface functional groups.

Therefore, the choice of these three samples enables us to investigate the role of pore structures

and surface areas in the BPD added electrolyte based Li-S cells. Moreover, the binder-free

nanofiber mat serves as a simple model cathode design preventing potential losses in pore

accessibility by binders and allows better interpretation of the effect of porosity.

We prepared CNFs/S, mi-CNFs/S, and me-CNFs/S cathodes using a rapid melt

sulfur infiltration technique recently developed in our group.[23] Briefly, a given amount of

sulfur was sprinkled homogeneously across the top of punched disk electrodes (11 mm
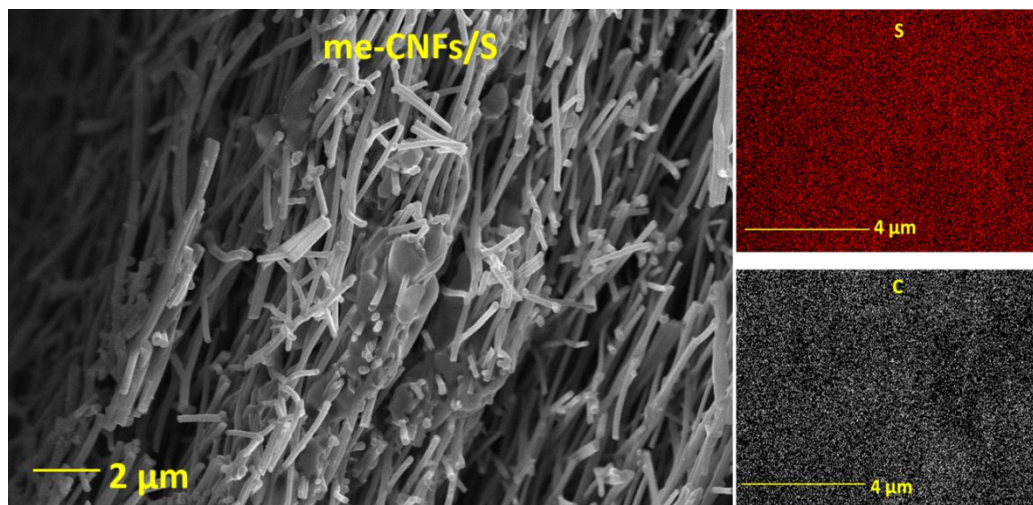

Fig. 2 Cross-sectional SEM image and elemental maps for the me-CNFs/S cathode.

diameter) and then heat pressed at 155°C for 50 sec at a mild pressure (≤250 psi). This

rapid heating using hydraulic heat press (preheated at 155°C) allows sulfur to diffuse

throughout the nanofiber mats.

The content of the sulfur was kept ~47-53 wt% (S loading of 1.3-1.5 mg cm^{-2}) in

final CNFs/S, mi-CNFs/S, and me-CNFs/S cathodes. The cross-sectional SEM image of

the me-CNFs/S electrode after sulfur infiltration and elemental maps for C and S elements

are given in figure 2. It is evident from the elemental maps that sulfur is evenly distributed

along the thickness of the nanofiber mats. Figure 3(a) and 3(b) show the thermogravimetric analysis (TGA) curves and derivative of weight% for the fabricated CNFs/S, mi-CNFs/S, and me-CNFs/S cathodes. The CNFs/S cathode exhibits a steep weight loss between 90°-185°C with a maximum at ~164°C (figure 3(b); region I).[26] As discussed above, the CNFs sample has a low surface area. The observed sharp sulfur loss indicates that the sulfur is mostly infiltrated in the inter-fiber macropores/voids in CNFs/S (region I). The mi-CNFs/S sample shows two weight loss peaks- one sharp weight loss at a temperature close to 150°C and second over a wide temperature range (150-300°C). The first sharp weight loss is attributed to sulfur present within inter-fiber macropores (region I) and the second gradual weight loss is possibly due to the sulfur confined in the micropores of mi-CNFs/S sample (region III). We estimate that 24-25% of the total infiltrated sulfur is confined within micropores and the rest is accommodated by inter-fiber macropores/voids.
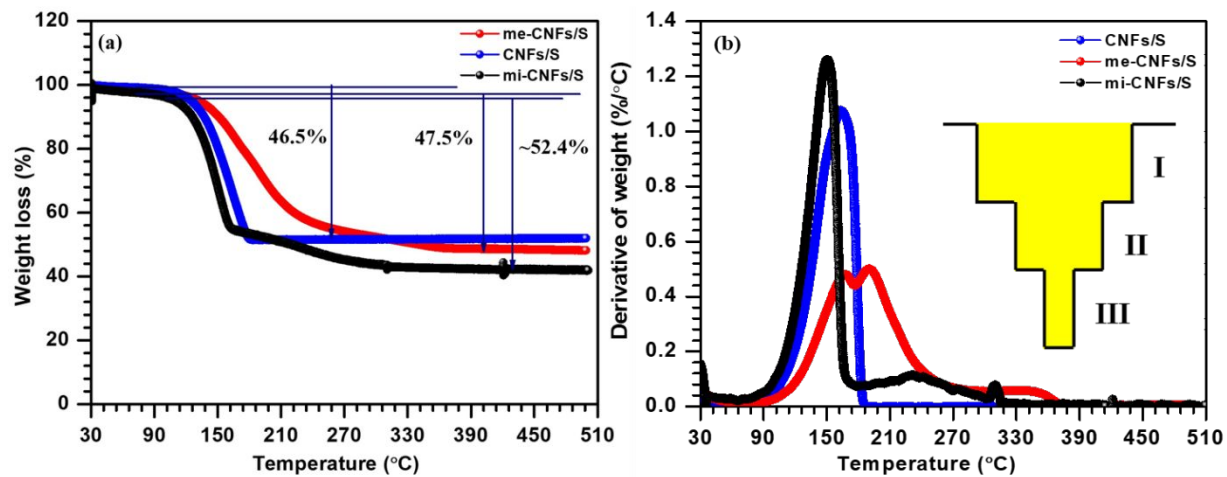
Fig. 3 (a) TGA curve and (b) derivative of weight % for CNFs/S, mi-CNFs/S and me-CNFs/S cathodes.

The me-CNFs/S cathode exhibits three distinctive temperatures for sulfur loss with a maximum at ~165°C, 190°C, and 350°C respectively (figure 3(b)). The first weight loss temperature, ~165°C, matches with the peak temperature observed in the CNFs/S cathode and is attributed to sulfur infiltrated (outside the fiber surface) within inter-fiber spacing/voids as mentioned earlier (region I).[26] The second weight loss maximum is observed around 35°C later, which represents an increased difficulty level for the sulfur possibly infiltrated within the mesopores (region II).[26] The third weight loss peak possibly

represents sulfur infiltrated deep inside the mesopores and micropores (region III).[26-27]As

seen in the TGA curve in figure 3(a), the weight loss in me-CNFs/S is gradual (rather than

sharp) even in the lower temperature range below 200°C, possibly due to the cumulative

effect of sulfur confined within mesopores and inter-fiber macropores. We estimate that

~80% of sulfur weight is lost within this temperature range. Mesopores are well known for

mass transportation thus help sulfur to reach deep inside micropores during the

preparation of me-CNFs/S cathodes at 155°C (50 seconds).[25]

For electrochemical testing, we fabricated 2032 coin-type Li-S cells using CNFs/S,

mi-CNFs/S, and me-CNFs/S cathodes in BPD added ether-based electrolyte (see more

details in the experimental section). Figure 4(a) shows charge-discharge curves for 10,

50, 100, 150 and 200th cycle collected at the C/2 rate for me-CNFs/S cathodes in BPD

additive based electrolyte. These discharge curves show two plateaus at around ~2.35 V

and ~2.0 V, which are attributed to the typical two-step reduction of sulfur to Li_2S_2/Li_2S

($S_8 \rightarrow Li_2S_x$; $4 \leq x \leq 8 \rightarrow Li_2S_2/Li_2S$). To evaluate the importance of me-CNFs/S cathodes,

we cycled CNFs/S (with BPD), mi-CNFs/S (with and without BPD) and me-CNFs/S

cathodes (with and without BPD) at a C/2 rate as shown in figure 4(b). The mi-CNFs/S

cathode-based Li-S (without BPD) cells show an initial specific capacity of ~851 mAh g^{-1}

which is decreased to ~767 mAh g^{-1} and ~243 mAh g^{-1} over 100 and 200 cycles,

respectively. The me-CNFs/S cathode-based Li-S (without BPD) cells exhibit an initial

specific capacity of ~964 mAh g^{-1} which is significantly reduced to ~592 mAh g^{-1} and ~61

mAh g^{-1} over 100 and 200 cycles, respectively. As expected, the relatively slower capacity

decay in mi-CNFs/S sample (compared to me-CNFs/S) is a result of confinement effect

of micropores that can better accommodate the small sized-polysulfides formed during

the redox reactions.[28-29] The slightly higher initial capacity of me-CNFs/S could be due to

its larger surface area providing a greater initial interfacial (carbon-sulfur) contact area for
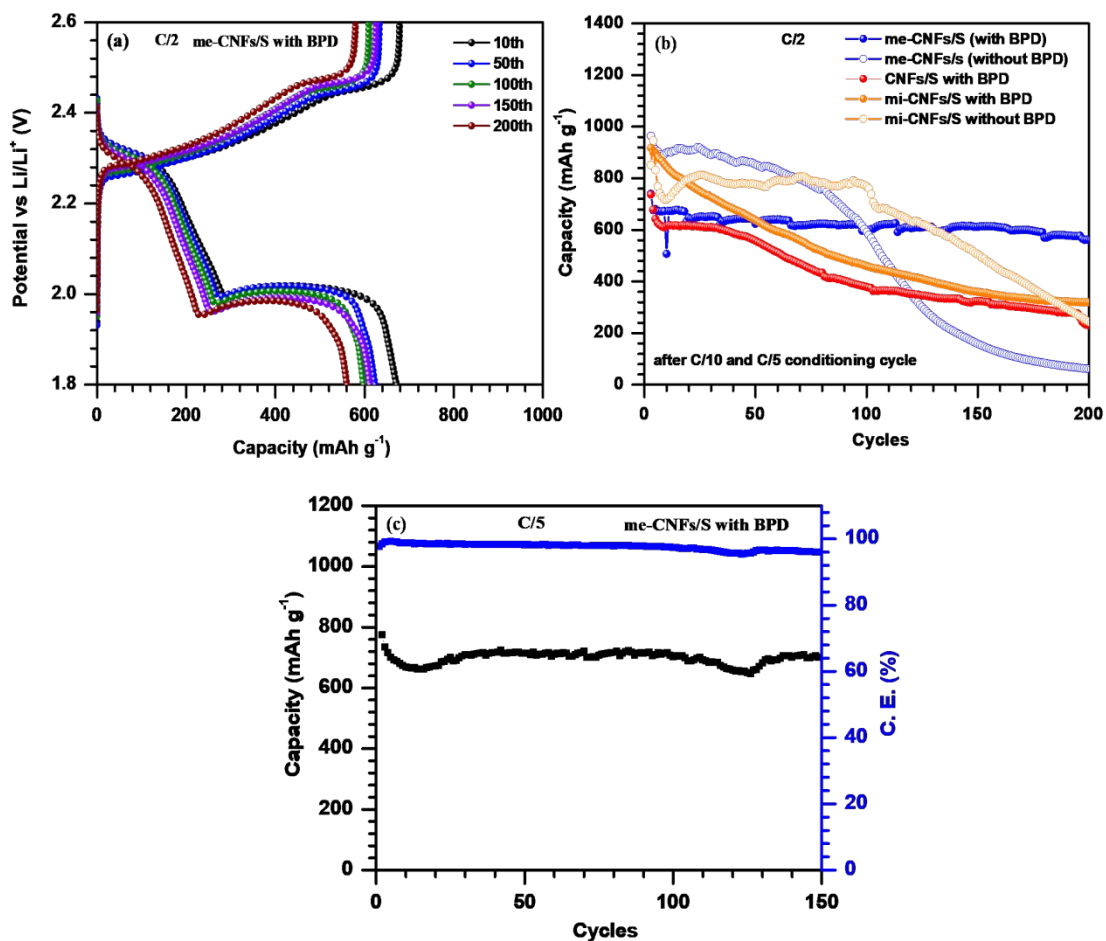
sulfur utilization.

Fig. 4 (a) Typical charge-discharge curves for me-CNFs/S cathode based Li-S cells in

BPD added electrolyte (b) long-term cycling for CNFs/S (with BPD), mi-CNFs/S (with

and without BPD) and me-CNFs/S cathodes (with and without BPD) based Li-S cells

20

and (c) long-term cycling at C/5 rate for me-CNFs/S cathode based Li-S cells in BPD

added electrolyte.

In the case of BPD added electrolyte, the capacity of the non-porous CNFs/S and

mi-CNFs/S cathodes drops very rapidly and is considerably decreased within 100 cycles.

The slightly higher initial capacity in mi-CNFs/S compared to CNFs/S cathode could be

due to the higher surface area. However, the fast decay suggests that the micropores in

mi-CNFs are not able to successfully confine the intermediate products. It is also worth

noting that this capacity decay in mi-CNFs/S cathodes with BPD added electrolyte is even

faster compared to that in the blank electrolyte (without BPD) (see figure 4(b)). In contrast,

me-CNFs/S based Li-S cells in BPD-based electrolyte show a stable capacity up to 200

and 150 cycles at C/2 (figure 4(b)) and C/5 (figure 4(c)) rates, respectively. Specifically,

it exhibits an initial capacity of 739 mAh g^{-1}. After an initial drop to 676 mAh g^{-1}in the first

cycle (possibly due to large aggregates of sulfur in inter-fiber spacing), the capacity

remains stable with 83% retention after 200 cycles. Similarly, at C/5, these samples

exhibit an initial capacity of 774 mAh g^{-1} with 90% retention after 150 cycles. The relatively

low initial capacity of me-CNFs in BPD-based electrolytes than in the blank electrolyte is

possibly due to alteration in the reaction pathway through the complex formation, which

can ultimately affect redox kinetics.[20] It is noteworthy that me-CNFs/S exhibit a lower initial

capacity than mi-CNFs/S in BPD added electrolyte, which is possibly due to a slight difference in

the distribution of sulfur into CNFs (Figure 3). The long-term cycling of me-CNFs/S cathodes

with BPD in comparison to me-CNFs/S cathodes without BPD is in good agreement with

the previous report because BPD tends to form complexes with short-chain intermediate

lithium polysulfides and suppress their dissolution and shuttling.[20] However, the BPD-S_x^{2-}

complex formation is expected to be similar in all three cathode systems, and complex

formation alone doesn't explain the performance deterioration in BPD-based mi-CNFs/S

cathodes (compared to blank electrolyte). We hypothesize that the porosity and surface

area of the nanofibers are playing an important rolein these Li-S cells and there is a need

to re-evaluate the optimum carbon host pore sizes in BPD-based electrolyte systems.

Biphenyl-4,4'-dithiol (BPD) molecules have two thiol functional (-SH) groups at

4,4'-positions of conjoined benzene rings which are attached through their 1,1'-positions

as shown in figure 5.[20] The presence of two –SH groups makes these neutral biphenyl

compound very reactive. As reported by H. –L., Wu *et al.*, these BPD molecules tend to

form complex with intermediate short-chain lithium polysulfides (S_x^{2-}) and suppress their

dissolution and shuttling.[20] The complex anion [BPD-S_x^{2-}] formation takes place through

S-S coupling between terminal sulfur (S_T) of the polysulfide S_x^{2-} anion and $-\dot{S}$ of the –SH
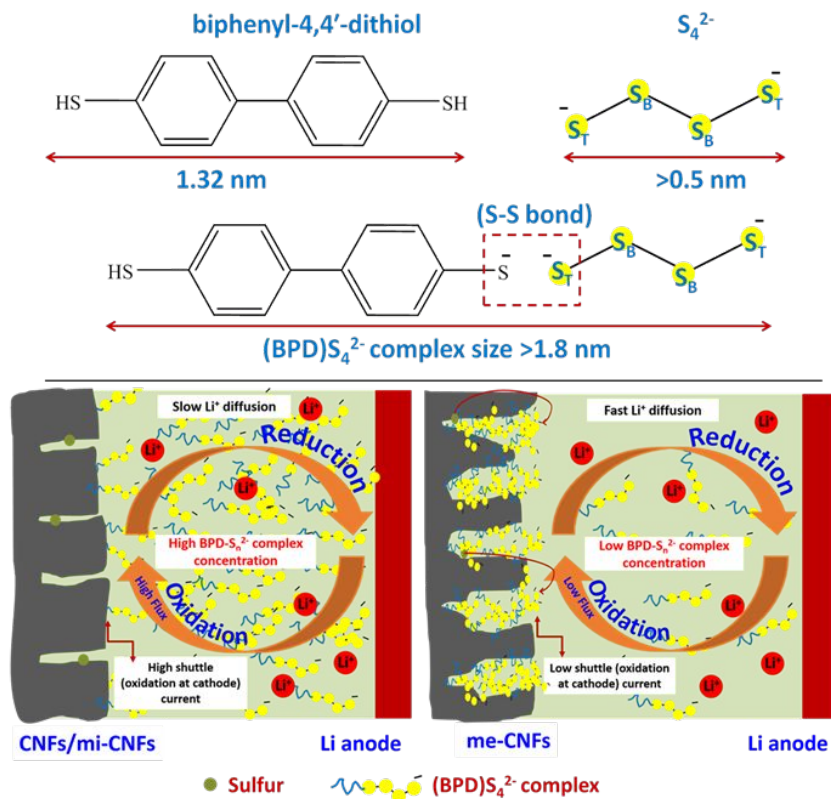
group of BPD as shown in figure 5.

Fig. 5 BPD-polysulfide complex size and a possible scheme explaining the role of porosity of carbon nanofibers in BPD added Li-S batteries.

As reported by L. G. Rosa *et al.*, the calculated dimension of the BPD molecule is ~1.32 nm.[30] On the other hand, short chain polysulfide anions viz., $\dot{S}_3^-$ radical or S_4^{2-} have dimensions ≥0.5 nm.[27, 31] Based on their individual sizes, we can infer that BPD complexes with short-chain polysulfide anions have dimensions >1.8 nm. Therefore, we believe that the carbon host at the cathode not only needs a high surface area but also needs pore sizes larger than the dimension of these BPD-polysulfide complexes for

successful complex adsorption, prevention of their migration to the Li-anode and stable

sulfur utilization. Otherwise, these complexes will still diffuse into the electrolyte and result

in undesired corrosion reactions on the lithium anode. Hence, me-CNFs/S with a high

surface area of 679 m^2/g and a large fraction of mesopores between 2.4-5.1 nm provides

the most stable capacity compared to mi-CNFs/S (high surface area with micropores) and

CNFs/S (low surface area). To further support our hypothesis that me-CNFs provide large

contact area and suitable porosity for adsorption of BPD complexes, we used two

approaches- Li^+ diffusion coefficient estimation and shuttle current measurements.

Measuring the Li^+ diffusion coefficient can provide useful qualitative information about the

concentration of BPD complexes into the electrolyte and ultimately the adsorption

capability of CNFs, mi-CNFs, and me-CNFs. A lower concentration of BPD-S_x^{2-}

complexes into the electrolyte will result in faster Li^+ diffusion and vice versa as depicted

in the schematic in figure 5. A series of cyclic voltammetry (CV) measurements were

performed at different scan rates for CNFs/S, mi-CNFs/S and me-CNFs/S cathodes

based Li-S cells in BPD added electrolyte to evaluate Li^+ diffusion coefficients, as shown

in figure 6(a-c). Two cathodic peaks at ~2.35 V and 2.0 V and one anodic peak at ~2.4 V

are denoted as A, B, and C, respectively. As shown in figure 6 (c-e), peak currents (I_p) are linear *w.r.t.* the square root of scan rates for all three A, B and C peaks, from which the Li$^+$ diffusion coefficient can be calculated using the classical Randles Sevcik equation(1) given below[32]:

$$I_p = (2.69 \times 10^5)n^{1.5}AD^{0.5}v^{0.5}C_0^*$$

(1)

Where I_p is the peak current in ampere, n is the number of electron transfer per reaction species; A is the electrode area in cm^2, v is the scan rate in Vsec^{-1}, D is the Li$^+$ diffusion coefficient in cm^{2}sec^{-1}, C_o^* is the bulk concentration in molcm^{-3}.[32] For a given A (0.855 cm^2), n (2), and C_o^* (0.00185 molcm^{-3}), the peak current is directly proportional to the square root of scan rate.
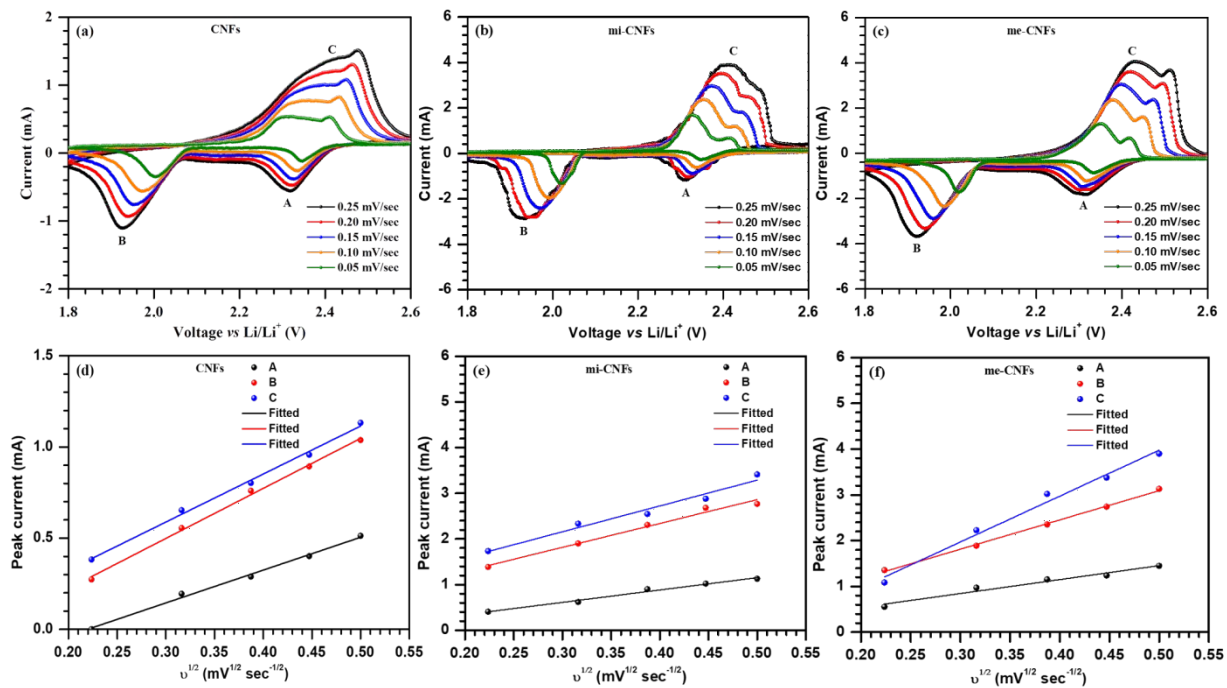
Fig. 6 CV curves collected at different scan rates for (a) CNFs/S, (b) mi-CNFs/S and (c) me-CNFs/S cathodes; peak currents vs. square root of scan rates at peak position A, B and C for (d) CNFs/S, (e) mi-CNFs/S and (f) me-CNFs/S based Li-S batteries in BPD added electrolyte.

The Li$^+$ diffusion coefficient D$_{Li+}$ can be calculated from the slope of the I_p vs. $v^{1/2}$ plot.[32] The calculated Li$^+$ diffusion coefficient values are summarized in Table 1.

Table 1. Calculated Li$^+$ diffusion coefficient for CNFs/S, mi-CNFs/S, and me-CNF/S cathodes.

Sample	D_{Li+} A (cm^{2}sec^{-1})	D_{Li+} B (cm^{2}sec^{-1})	D_{Li+} C (cm^{2}sec^{-1})
CNFs/S	2.24E-09	5.21E-09	4.77E-09
mi-CNFs/S	5.07E-09	1.89E-08	1.22E-08
me-CNFs/S	6.41E-09	2.83E-08	6.95E-08

It is evident that compared to the CNFs/S and mi-CNFs/S cathodes, values of Li$^+$

diffusion coefficients are higher for me-CNFs/S cathodes, which suggests a lower

concentration of polysulfide-BPD complexes in the electrolyte solution. The observed

faster Li$^+$ diffusion for me-CNFs/S cathodes is in good agreement with the cycling data

and further supports our hypothesis given in figure 5. The enhancement in Li$^+$ diffusion

coefficients is found to be more prominent at B and C positions since BPD forms

complexes mainly with lower order polysulfides (at B and C, we have more concentration

of these complexes).[20]

The second approach we used to substantiate our hypothesis is the measurement

of shuttle current at a given S-loading, and state-of-charge potential for mi-CNFs/S and

me-CNFs/S cathodes based Li-S cells in BPD added electrolyte. Since LiNO$_3$ is an anti-

agent for shuttling process[13], we used BPD added electrolyte without the addition of

LiNO$_3$ for shuttle current measurements. In the shuttling process, the potential of the

cathode decreases steadily due to the oxidation of continuously arriving lower-order

polysulfides (generated at the anode) towards the cathode as shown in figure 5.[33-

36]However, if we maintain the cathode at a constant state-of-charge potential (~2.3V in

this case) by the passage of external electric current, the flux involved in the shuttle

process would also hold a constant value. The externally applied current will counter

balance the oxidation current generated at the cathode due to the constant flux involved

in the shuttle process and maintain the cathode at the given state-of-charge potential.

This required external current can then be used to estimate the shuttle current, i.e.,

oxidation current generated at the cathode for a given state-of-the charge potential.[33-36]

The shuttle-current measurements were performed at ~2.3 V during the 3rd

charging process (i.e., 3rd cycle after two full cyclic voltammetry scans). At this voltage, the

concentration of lower order polysulfides (and therefore BPD complexes) is expected to

be high since the conversion of these lower order polysulfides to long chain polysulfides

is incomplete. Li-S cells were held at this voltage for 30 minutes to equilibrate cells before
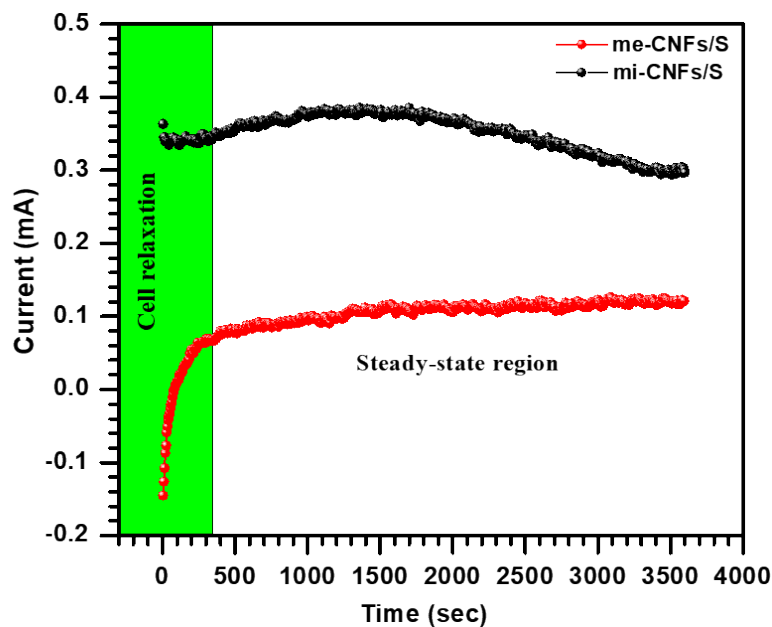
measuring the shuttle current.

Fig. 7 Steady-state shuttle current measured for mi-CNFs/S and me-CNFs/S cathode-

based Li-S cells in BPD added electrolyte (without $LiNO_3$).

In figure 7, we can see that the cell relaxation time for mi-CNFs/S and me-CNFs/S cathode

is different, which is possibly due to the difference in the flux involved.[33-36] The lower steady-state

shuttle current observed for the me-CNFs/S cathode in comparison to mi-CNFs cathodes indicates

a relatively lower BPD-polysulfide flux involved in the oxidation process at the me-CNFs/S

cathodes (figure 5). This result further supports that a low concentration of BPD complexes is

present in the electrolyte and that me-CNFs provide a relatively stronger adsorption capability. It

is evident from the Li^+ diffusion coefficient and shuttle-current measurements that micro-

mesoporous me-CNFs are the more suitable host for sulfur than non-porous CNFs and micro-

porous mi-CNFs for BPD additive based electrolyte in Li-S batteries. Therefore, texture properties–surface area and porosity of the conducting host materials cannot be neglected while designing functional additive based electrolytes for Li-S batteries.

Conclusions

In summary, we compared the electrochemical performance of Li-S cells fabricated with non-porous carbon nanofibers (CNFs/S), microporous carbon nanofibers (mi-CNFs/S) and micro-mesoporous carbon nanofibers (me-CNFs/S) based sulfur cathodes in biphenyl-4,4'-dithiol (BPD) added electrolyte. We found that me-CNFs/S cathodes exhibit superior performance with a stable specific capacity of ~561mAh g^{-1} over 200 cycles at a C/2 rate. Diffusion coefficient measurements show that the me-CNFs/S based Li-S cells exhibit faster Li^+ ion diffusion during reduction and oxidation processes thus manifest a low concentration of BPD-complex species into the electrolyte. Moreover, the me-CNFs/S based Li-S cells show a relatively lower shuttle current in BPD added electrolyte in comparison to mi-CNFs/S cathodes. Based on the size of BPD-S_x^{2-} complex, our results demonstrate that the use of mesoporous me-CNFs is essential for achieving stable cycling in BPD added electrolyte based Li-S cells.

Conflicts of Interest

There are no conflicts to declare.

References

1.   Manthiram, A., Fu, Y., Chung, S. H., Zu, C. & Su, Y. S. Rechargeable Lithium-Sulfur Batteries. *Chem. Rev.* **114**, 11751-11787 (2014).

2.   Pang, Q., Liang, X., Kwok, C. Y. & Nazar, L. F. Advances in Lithium–Sulfur Batteries Based on Multifunctional Cathodes and Electrolytes. *Nat. Energy* **1**, 16132-16142 (2016).

3.   Borchardt, L., Oschatz, M. & Kaskel, S. Carbon Materials for Lithium Sulfur Batteries-Ten Critical Questions. *Chem. Eur. J.* **22**, 7324-7351 (2016).

4.   Hagen, M., Hanselmann, D., Ahlbrecht, K., Maça, R., Gerber, D. & Tübke, J. Lithium-Sulfur Cells: The Gap between the State-of-the-Art and the Requirements for High Energy Battery Cells. *Adv. Energy Mater.* **5**, 1401986-1401996 (2015).

5.   Muldoon, J., Bucur, C. B. & Gregory, T. Quest for Nonaqueous Multivalent Secondary Batteries: Magnesium and Beyond. *Chem. Rev.* **114**, 11683-11720 (2014).

6.   Seh, Z. W., Sun, Y., Zhang, Q. & Cui, Y. Designing high-energy lithium-sulfur batteries. *Chem. Soc. Rev.* **45**, 5605-5634 (2016).

7.   Wang, D.-W., Zeng, Q., Zhou, G., Yin, L., Li, F., Cheng, H.-M., Gentle, I. R. & Lu, G. Q. M. Carbon–sulfur composites for Li–S batteries: status and prospects. *J. Mater. Chem. A* **1**, 9382-9394 (2013).

8.   Park, J., Yu, S.-H. & Sung, Y.-E. Design of structural and functional nanomaterials for lithium-sulfur batteries. *Nano Today* **18**, 35-64 (2018).

9.   Liang, X., Kwok, C. Y., Lodi-Marzano, F., Pang, Q., Cuisinier, M., Huang, H., Hart, C. J., Houtarde, D., Kaup, K., Sommer, H., Brezesinski, T., Janek, J. & Nazar, L. F. Tuning

Transition Metal Oxide-Sulfur Interactions for Long Life Lithium Sulfur Batteries: The

"Goldilocks" Principle. *Adv. Energy Mater.* **6**, 1501636-1501645 (2016).

10.   Shanthi, P. M., Hanumantha, P. J., Gattu, B., Sweeney, M., Datta, M. K. & Kumta,

P. N. Understanding the Origin of Irreversible Capacity loss in Non-Carbonized Carbonate

− based Metal Organic Framework (MOF) Sulfur hosts for Lithium − Sulfur battery.

Electrochim. Acta **229**, 208-218 (2017).

11.   Xiao, L., Cao, Y., Xiao, J., Schwenzer, B., Engelhard, M. H., Saraf, L. V., Nie, Z.,

Exarhos, G. J. & Liu, J. A Soft Approach to Encapsulate Sulfur: Polyaniline Nanotubes

for Lithium-Sulfur Batteries with Long Cycle Life. *Adv. Mater.* **24**, 1176-1181 (2012).

12.   Zhang, S. S. Role of $LiNO_3$ in rechargeable lithium/sulfur battery. *Electrochim. Acta*

70, 344-348 (2012).

13.   Rosenman, A., Elazari, R., Salitra, G., Markevich, E., Aurbach, D. & Garsuch, A.

The Effect of Interactions and Reduction Products of $LiNO_3$, the Anti-Shuttle Agent, in

Li-S Battery Systems. *J. Electrochem. Soc.* **162**, A470-A473 (2015).

14.   Fei, H., An, Y., Feng, J., Ci, L. & Xiong, S. Enhancing the safety and electrochemical performance of ether based lithium sulfur batteries by introducing an efficient flame retarding additive. *RSC Adv.* **6**, 53560-53565 (2016).

15.   Thieme, S., Brückner, J., Meier, A., Bauer, I., Gruber, K., Kaspar, J., Helmer, A., Althues, H., Schmuck, M. & Kaskel, S. A lithium–sulfur full cell with ultralong cycle life: influence of cathode structure and polysulfide additive. *J. Mater. Chem. A* **3**, 3808-3820 (2015).

16.   Jia, L., Wu, T., Lu, J., Ma, L., Zhu, W. & Qiu, X. Polysulfides Capture-Copper Additive for Long Cycle Life Lithium Sulfur Batteries. *ACS Appl. Mater. Interfaces* **8**, 30248-30255 (2016).

17.   Wu, F., Thieme, S., Ramanujapuram, A., Zhao, E., Weller, C., Althues, H., Kaskel, S., Borodin, O. & Yushin, G. Toward in-situ protected sulfur cathodes by using lithium bromide and pre-charge. *Nano Energy* **40**, 170-179 (2017).

18.   Eshetu, G. G., Judez, X., Li, C., Bondarchuk, O., Rodriguez-Martinez, L. M., Zhang, H. & Armand, M. Lithium Azide as an Electrolyte Additive for All-Solid-State Lithium-Sulfur Batteries. *Angew. Chem. Int. Ed.* **56**, 15368-15372 (2017).

19.   Wu, F., Lee, J. T., Nitta, N., Kim, H., Borodin, O. & Yushin, G. Lithium iodide as a

promising electrolyte additive for lithium-sulfur batteries: mechanisms of performance

enhancement. *Adv. Mater.* **27**, 101-108 (2015).

20.   Wu, H.-L., Shin, M., Liu, Y.-M., See, K. A. & Gewirth, A. A. Thiol-based electrolyte

additives for high-performance lithium-sulfur batteries. *Nano Energy* **32**, 50-58 (2017).

21.   Tran, C. & Kalra, V. Fabrication of Porous Carbon Nanofibers with Adjustable Pore

Sizes as Electrodes for Supercapacitors. *J. Power Sources* **235**, 289-296 (2013).

22.   Singhal, R., Chung, S.-H., Manthiram, A. & Kalra, V. A free-standing carbon

nanofiber interlayer for high-performance lithium–sulfur batteries. *J. Mater. Chem. A* **3**,

4530-4538 (2015).

23.   Dillard, C., Chung, S.-H., Singh, A., Manthiram, A. & Kalra, V. Binder-Free,

Freestanding Cathodes Fabricated with an Ultra-Rapid Diffusion of Sulfur Into Carbon

Nanofiber Mat for Lithium Sulfur Batteries. *Mater. Today Energy* **9**, 336-344 (2018).

24.   Leofantia, G., Padovanb, M., Tozzolac, G. & Venturellic, B. Surface area and pore

texture of catalysts. *Catal. Today* **41**, 207-219 (1998).

25.   Singh, A. & Chandra, A. Enhancing Specific Energy and Power in Asymmetric

Supercapacitors - A Synergetic Strategy based on the Use of Redox Additive Electrolytes.

Sci. Rep. **6**, 25793-25805 (2016).

26.   Choi, H., Zhao, X., Kim, D.-S., Ahn, H.-J., Kim, K.-W., Cho, K.-K. & Ahn, J.-H. A

mesoporous carbon–sulfur composite as cathode material for high rate lithium sulfur

batteries. *Mater. Res. Bull.* **58**, 199-203 (2014).

27.   Xin, S., Gu, L., Zhao, N. H., Yin, Y. X., Zhou, L. J., Guo, Y. G. & Wan, L. J. Smaller

sulfur molecules promise better lithium-sulfur batteries. *J. Am. Chem. Soc.* **134**, 18510-

18513 (2012).

28.   Guo, J., Zhang, J., Jiang, F., Zhao, S., Su, Q. & Du, G. Microporous carbon

nanosheets derived from corncobs for lithium–sulfur batteries. *Electrochim. Acta* **176**,

853-860 (2015).

29.   Xu, Y., Wen, Y., Zhu, Y., Gaskell, K., Cychosz, K. A., Eichhorn, B., Xu, K. & Wang,

C. Confined Sulfur in Microporous Carbon Renders Superior Cycling Stability in Li/S

Batteries. *Adv. Funct. Mater.* **25**, 4312-4320 (2015).

30.   Rosa, L. G. & Liang, J. Atomic force microscope nanolithography: dip-pen, nanoshaving, nanografting, tapping mode, electrochemical and thermal nanolithography. *J. Phys. Condens. Matter.* **21**, 483001-483018 (2009).

31.   Scholz, J., Kayaalp, B., Juhl, A. C., Clemens, D., Fröba, M. & Mascotto, S. Severe Loss of Confined Sulfur in Nanoporous Carbon for Li–S Batteries under Wetting Conditions. *ACS Energy Lett.* **3**, 387-392 (2018).

32.   Tao, X., Wang, J., Liu, C., Wang, H., Yao, H., Zheng, G., Seh, Z. W., Cai, Q., Li, W., Zhou, G., Zu, C. & Cui, Y. Balancing Surface Adsorption and Diffusion of Lithium-Polysulfides on Nonconductive Oxides for Lithium-Sulfur Battery Design. *Nat. Commun.* **7**, 11203-11211 (2016).

33.   Diao, Y., Xie, K., Xiong, S. & Hong, X. Shuttle phenomenon – The irreversible oxidation mechanism of sulfur active material in Li–S battery. *J. Power Sources* **235**, 181-186 (2013).

34.   Hofmann, A. F., Fronczek, D. N. & Bessler, W. G. Mechanistic modeling of polysulfide shuttle and capacity loss in lithium–sulfur batteries. *J. Power Sources* **259**, 300-310 (2014).

38

35.   Mikhaylik, Y. V. & Akridge, J. R. Polysulfide Shuttle Study in the Li/S Battery

System. *J. Electrochem. Soc.* **151**, A1969-A1976 (2004).

36.   Moy, D., Manivannan, A. & Narayanan, S. R. Direct Measurement of Polysulfide

Shuttle Current: A Window into Understanding the Performance of Lithium-Sulfur Cells.

J. Electrochem. Soc. **162**, A1-A7 (2014).

Table of content:

Role of mesoporous carbon nanofibers as sulfur host is highlighted for efficient use of biphenyl-4,4'-dithiol electrolyte additive in Li-S batteries